Journal of Power Sources 213 (2012) 265–269

Contents lists available at SciVerse ScienceDirect

Journal of Power Sources

journal homepage: www.elsevier.com/locate/jpowsour

Short communication

Iron- and nitrogen-functionalized graphene as a non-precious metal catalyst for enhanced oxygen reduction in an air-cathode microbial fuel cell

Sizhe Li [a,b,1], Yongyou Hu [a,b,*], Qian Xu [a,b,2], Jian Sun [a,b,3], Bin Hou [a,b,4], Yaping Zhang [a,b,5]

[a] The Key Laboratory of Pollution Control and Ecosystem Restoration in Industry Clusters, Ministry of Education, School of Environmental Science and Engineering, South China University of Technology, Guangzhou 510006, China
[b] State Key Lab of Pulp and Paper Engineering, South China University of Technology, Guangzhou 510640, China

ARTICLE INFO

Article history:
Received 15 February 2012
Received in revised form
1 April 2012
Accepted 3 April 2012
Available online 13 April 2012

Keywords:
Microbial fuel cell
Graphene
Oxygen reduction reaction
Non-precious catalyst

ABSTRACT

In this work, iron- and nitrogen-functionalized graphene (Fe–N–G) as a non-precious metal catalyst is synthesized via a facile method of thermal treatment of a mixture of Fe salt, graphitic carbon nitride (g-C_3N_4) and chemically reduced graphene. The electrocatalytic activity of the prepared catalysts toward oxygen reduction reaction (ORR) evaluated by using linear sweep voltammetry tests shows that the Fe–N–G catalyst has more positive onset potential and increased reduction current densities as compared to the pristine graphene (P–G) catalyst, indicating an enhanced ORR activity of the Fe–N–G catalyst. More importantly, the Fe–N–G-MFC achieves the highest power density of 1149.8 mW m^{-2}, which is ~2.1 times of that generated with the Pt/C-MFC (561.1 mW m^{-2}) and much higher than that of the P–G-MFC (109 mW m^{-2}). These results demonstrate that the Fe–N–G catalyst can hold the promise of being an excellent alternative to the costly Pt catalyst for practical MFC applications.

1. Introduction

Microbial fuel cell (MFC) is a well-known system that exploits microbial activities to harvest energy from organic or inorganic matter [1–3]. In a MFC, substrate is oxidized by microorganisms and electrons subsequently transferred to the cathode via the external circuit. Various oxidants can be used as cathodic electron acceptors, among which oxygen is the most favorable acceptor for its sustainability [4]. One critical issue to be addressed is the development of effective electrocatalysts for oxygen reduction reaction (ORR) to facilitate power output in MFCs. Platinum (Pt) and Pt-based materials are extensively utilized as air-cathode catalysts for ORR, but Pt is expensive, rare and sensitive toward catalyst poisoning which diminishes the performance of MFCs and hinders its practical application [5]. Therefore, aiming to reduce the usage of the precious Pt and accordingly the cost of an MFC, the exploitation of cheap and more active non-precious metal ORR electrocatalysts is intensively pursued by researchers around the world [6–16].

Graphene, emerging as a true two-dimensional material, has attracted wide-ranging attention for application in the next generation electronic devices [17]. Owing to intrinsically superior electrical conductivity, excellent mechanical flexibility, high surface area, as well as ease of functionalization, graphene provides an ideal base for nanoelectronics [18], energy storage materials [19,20], biosensing [21], and catalysts [22]. Theoretical [23] and detailed experimental [24,25] studies have shown that functionalization or chemical doping with foreign atoms are effective approaches to tailor the chemical and physical properties of graphene. Recent studies have suggested that nitrogen-doped graphene (N–G) can enhance the conductivity of graphene and its electrocatalytic activity as well [22,26]. Very recently, Feng et al. [27] reported a nitrogen-doped graphene catalyst applied in MFCs, which presented a comparable electrocatalytic activity for ORR and less expensive compared with the Pt catalyst. Nevertheless, the synthetic precursors of cyanuric chloride and trinitrophenol used in the detonation procedure are toxic or highly explosive. In addition, the ORR process of N–G in neutral medium (widely used in MFCs) is a combination of two-electron and four-electron pathways [27].

* Corresponding author. School of Environmental Science and Engineering, South China University of Technology, Guangzhou 510006, China. Tel.: +86 20 39380506; fax: +86 20 39380508.
E-mail addresses: scutlsz@gmail.com (S. Li), ppyyhu@scut.edu.cn (Y. Hu), fenglingxq@gmail.com (Q. Xu), sunjian472@163.com (J. Sun), houbin566@163.com (B. Hou), zhang.yp@mail.scut.edu.cn (Y. Zhang).
[1] Tel.: +86 15989036737.
[2] Tel.: +86 15013030126.
[3] Tel.: +86 20 39383779.
[4] Tel.: +86 15914305840.
[5] Tel.: +86 15920480187.

0378-7753/$ – see front matter © 2012 Elsevier B.V. All rights reserved.
doi:10.1016/j.jpowsour.2012.04.002

As is known, two-electron pathway is not only competing with four-electron pathway but also yielding undesirable hydrogen peroxide that is corrosive and can cause damages to membrane or electrode materials in fuel cells [28,29]. According to a recent report, researchers have demonstrated that the fast disproportionation of hydrogen peroxide can be facilitated by iron center in the pyrolyzed catalysts [30]. Previous study has revealed that carbon-based catalysts with iron coordinated to heterocyclic nitrogen (N) exhibit superb performance in polymer electrolyte fuel cells [31]. Thus, catalyst based on functionalized graphene with iron and nitrogen can be a promising candidate for ORR in neutral pH condition. Although investigation of such a functionalized graphene catalyst involving ORR in acid has been proposed [32], to our knowledge, the use of iron- and nitrogen-functionalized graphene (Fe–N–G) as cathodic catalyst in MFC has not yet been reported.

In the present study, the Fe–N–G catalyst was synthesized by a facile thermal method. X-ray photoelectron spectroscopy (XPS) was employed to identify different elements and various nitrogen functional groups. The electrocatalytic activities of the Fe–N–G catalyst were studied using linear sweep voltammetry (LSV), compared to that of the pristine graphene and commercial Pt/C catalyst. Then, the performance of MFCs with these catalysts modified cathodes was evaluated in terms of power densities and polarization behaviors of individual electrode.

2. Experimental

2.1. Synthesis of graphene oxide and catalyst

Graphene oxide (GO) was prepared from graphite powder (Sinopharm Chemical Reagent Co., Ltd., China) using modified Hummers methods [33,34]. In detail, graphite powder (5 g) and $NaNO_3$ (5 g) were mixed with concentrated H_2SO_4 (125 mL, 98 wt %) in an ice bath. With continuous agitation, 15 g of $KMnO_4$ was slowly added to the above mixture to prevent the temperature of the suspension from exceeding 20 °C. The mixture was stirred at 35 °C until it became pasty brownish (~2 h) and then diluted with slow addition of 250 mL of water. Subsequently, the suspension was diluted by 350 mL of water and treated with a H_2O_2 solution (30 mL, 30%). The resultant bright-yellow suspension was washed with HCl (1000 mL, 5%) and water several times, followed by centrifugation (16 000 rpm for 5 min) and careful washing to clean out remnant salt. After that, the product was dried in a vacuum oven at 60 °C for 24 h. As synthesized graphite oxide was dispersed in water to create a 1.25 mg mL^{-1} suspension, which was subjected to sonication (300 W) for 1 h to obtain GO. Ultrapure Milli-Q water was used in above experiments.

The detailed experimental procedure [32] for the preparation of the catalyst is described as follows. The g-C_3N_4 precursor was synthesized by thermal polymerization of dicyandiamide (Aladdin, China) at 550 °C using a tube furnace with a flow of argon [35]. For the preparation of the Fe–N–G catalyst, 0.025 g of $FeCl_3$ and 0.25 g g-C_3N_4 were mixed in deionized (DI) water and then heat up to 80 °C, followed by adding 100 mL of GO suspension (1.25 mg mL^{-1}). Under vigorous stirring, 350 μL of NH_3 (25%) and 50 μL of hydrazine hydrate (50%) were sequentially heated at 100 °C. The mixture was kept stirring at 130 °C until the solution completely evaporated and then collected and ground with a mortar and pestle. As-obtained powder was placed in the center of a quartz tube under argon flow. The temperature of tube furnace was elevated to 800 °C at a rate of 20 °C min^{-1} and held at 800 °C for 2 h. After cooling to room temperature, the sample was acid-leached in 2 M H_2SO_4 at 80 °C for 3 h. In contrast, pristine graphene was prepared by a similar procedure in the absence of $FeCl_3$ or g-C_3N_4, which was denoted as P–G.

2.2. Electrodes preparation

Air-cathode was made of carbon paper (5 cm × 5 cm) with PTFE waterproof layers described by Cheng et al. [36]. For catalyst layer, 12.5 mg of Fe–N–G powder was sonicated in a mixture of 87.5 μL Nafion (5%) and 0.5 mL absolute ethanol for 30 min, and then the dispersion was coated onto the as-prepared carbon paper followed by drying at room temperature overnight. For comparison, P–G and commercial Pt/C (40%, Hesen, China) were applied to each cathode using the same method. To investigate the electrocatalytic activity of ORR, a glassy carbon electrode (GCE, 3 mm in diameter) was modified with catalyst solution coated onto its surface. All the catalysts were prepared with a loading of 0.5 mg cm^{-2}.

2.3. MFC setup and operation

An air-cathode single-chamber MFC was constructed as previously described [37,38], consisting of cylindrical anode chamber (5 cm in diameter, 2.2 cm in length; effective volume of 40 mL), cation exchange membrane (Zhejiang Qianqiu Group Co., Ltd. China) and carbon felt electrode (anode; projected surface area of 10.2 cm^2). Prior to use, both carbon felt and carbon paper were cleaned by soaking in acetone overnight and then washed thoroughly with DI water. The catalyzed cathode was placed at a distance of 1 cm from the anode with the waterproof layer facing to air. MFCs were inoculated with anaerobic activated sludge collected from Liede municipal wastewater treatment plant, Guangzhou, China. The anodic medium contained: 0.5 g L^{-1} of sodium acetate, a phosphate buffer solution (PBS, 50 mM), a mineral solution (12.5 mL L^{-1}) and a vitamin solution (12.5 mL L^{-1}) [39], which was periodically refreshed when the voltage dropped below 20 mV. Titanium wires were used to connect the circuit with an external resistance of 500 Ω. All experiments were carried out in duplicate at room temperature (30 ± 1 °C), and average values with standard deviation were reported.

2.4. Analysis and calculations

The voltage of each MFC was recorded every 10 min with a data acquisition system (Model 2700, Keithly Instruments, USA). For current–voltage analysis, MFCs were allowed to equilibrate at open circuit for ~4 h, until the open circuit voltage (OCV) of each MFC stabilized. Then the polarization data were measured by varying an external resistor in the range of 2000–50 Ω (The time required for establishment of steady OCV for all the tested MFCs is approximately the same.). The anode and cathode potentials were measured by placing a saturated calomel electrode (SCE, +0.242 V vs. standard hydrogen electrode (SHE)) in the anode chamber for reference. Current density (mA cm^{-2}) was calculated from $I = U/(RA)$, and power density (mW m^{-2}) was calculated from $P = UI/A$, where U (V) is the cell voltage, and A (cm^{-2}) is the projected area of the cathode.

The morphology of Fe–N–G and P–G samples was characterized with a field emission scanning electron microscope (FESEM, Nova NanoSEM 430, FEI, USA). Raman spectra were carried out on a LabRAM Aramis (Horiba Jobin Yvon, France) with 632.8 nm laser excitation. XPS measurements were performed on an ESCALAB 250 with Al Kα radiation (15 kV, 150 W).

All electrochemical measurements were conducted on a PARSTAT 2273 potentiostat. LSV were tested in 50 mM PBS using a conventional three-electrode setup comprising a saturated calomel electrode (SCE) as reference, Pt foil as counter and catalyst-modified GCE (or bare GCE) as working electrode.

3. Results and discussion

3.1. Characterization of graphene-based catalyst

The morphologies of as-prepared catalyst were presented in Fig. 1. Fig. 1A shows the representative FESEM image of graphene sheets. It can be seen that P–G exhibited a typical aggregated and wrinkled structure. As shown in Fig. 1B, comparatively similar morphology of Fe–N–G was observed, showing additional ribbon-like areas. These differences are possibly owing to the functionalization process.

Raman spectroscopy is a widely used technique to characterize the properties of carbon materials and in particular disorder and defect structures [40]. As can be seen in Fig. 2c, two characteristic peaks of graphite at $\sim$1330 cm^{-1} and $\sim$1580 cm^{-1} have been assigned to the D band and G band, respectively. The intensity of the D band is strongly associated with the disorder degree of carbon, while the G band is attributed to the E_{2g} mode of the in-plane sp^2 domains, corresponding to ordered carbon atoms.

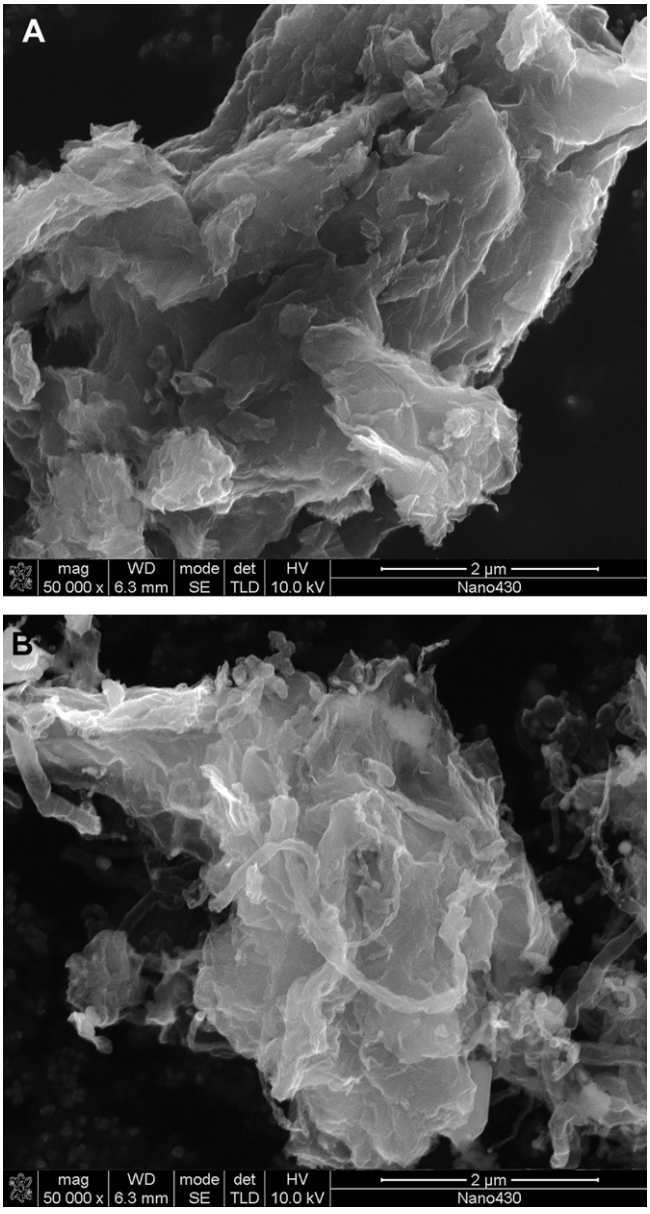

Fig. 1. FESEM images of (A) P–G and (B) Fe–N–G.

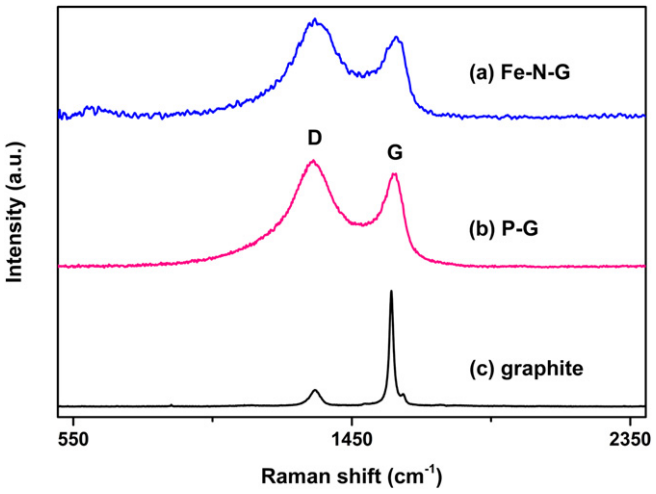

Fig. 2. Raman spectra of (a) Fe–N–G, (b) P–G and (c) graphite.

In contrast, the intensity of the D band was populated for P–G (Fig. 2b), owing to the increased number of edge sites as the lateral dimensions decreased [41]. The I_D/I_G ratio of Fe–N–G (1.22) was found to be higher than that of P–G (1.14), revealing that functionalized graphene is more disordered than the pristine graphene [42–44]. The increase in I_D/I_G should be caused by the addition of iron and nitrogen [45], demonstrating the successful functionalization of graphene-based catalyst.

To determine the chemical compositions of prepared catalysts, XPS analysis was performed. From the survey spectra (Fig. 3A), a predominant narrow C1s peak at 284.8 eV, along with an N1s peak at 398 eV for both Fe–N–G and P–G samples. In addition to the C1s and N1s peaks, a Fe2p3 peak at 710.66 eV was observed, which confirmed that iron and nitrogen were successfully incorporated into the graphene sheets (Fig. 3A). A weak N1s peak was also presented for pristine graphene, possibly due to the employed NH_3 during the synthetic procedure [46]. The high resolution N1s peaks in the XPS spectra of Fe–N–G were fitted into four components originating from pyridinic N (398.5 eV), pyrrolic N (399.8 eV), graphitic N (401.3 eV) and oxidized N (403.6 eV) (Fig. 3B) [32,47].

3.2. Oxygen reduction activities of the catalysts

LSV tests were conducted to investigate the electrocatalytic activity of the Fe–N–G catalyst for ORR in O_2-saturated 50 mM PBS medium. As shown in Fig. 4, featureless peak at the P–G electrode was observed, whereas the Fe–N–G electrode exhibited a pronounced electrocatalytic behavior toward O_2 reduction with increased current densities (-0.91 mA cm^{-2}) and a more positive onset potential (where the ORR commenced) at around 0.22 V (vs. SCE). This positive potential shift of the functionalized graphene implies an enhanced catalytically activity (kinetically more facile) for O_2 reduction. As discussed in Section 3.1, pyridinic N, pyrrolic N and graphitic N are presented at the graphene surface, all of which can efficiently create ORR active sites [48,49]. It is believed that carbon atoms adjacent to nitrogen dopants possess a substantially high positive charge density to counterbalance the strong electronic affinity of the nitrogen atom [48]. The nitrogen-induced charge delocalization could also alter the adsorption behavior of graphene toward oxygen, which effectively weaken the O–O bonding to facilitate the ORR process [48]. Furthermore, the addition of iron in the graphene-based catalyst can stabilize the incorporation of nitrogen within the graphene matrix, promoting electron transfer for O_2 reduction [50,51]. It has also been found

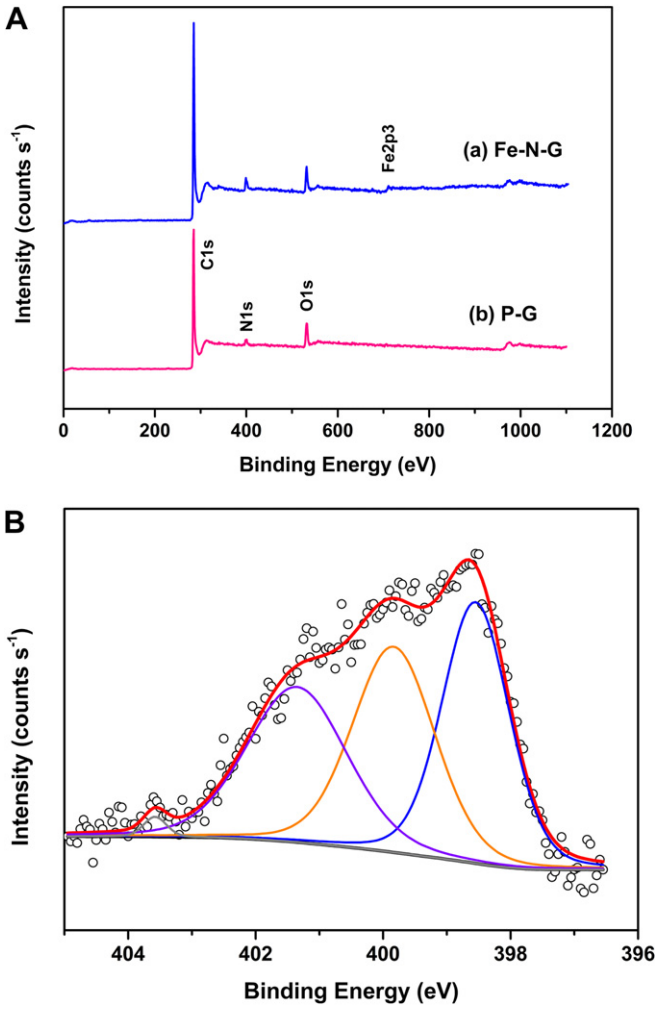

Fig. 3. (A) XPS survey of (a) Fe–N–G, (b) P–G; (B) high resolution N1s spectra of Fe–N–G.

that iron can also facilitate the fast disproportionation of undesirable hydrogen peroxide, which may accordingly promote the ORR process through a four-electron reduction pathway to produce water [30]. For comparison, although the Pt/C electrode showed a higher current response than the Fe–N–G electrode toward ORR, the power output of each MFC displayed dissimilar trend as presented in the following section.

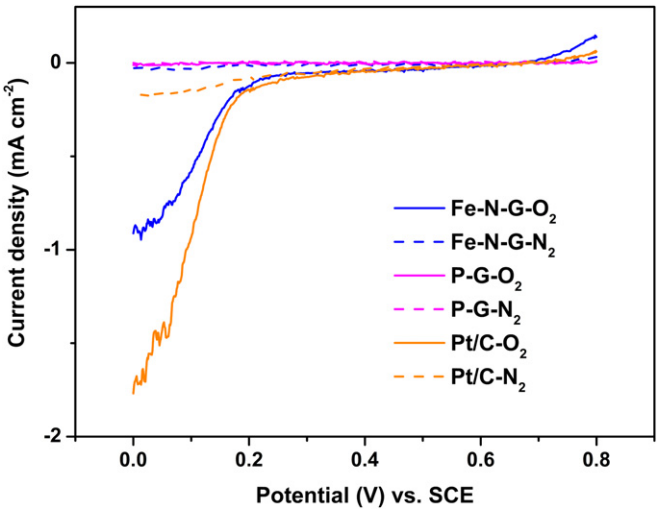

Fig. 4. LSV curves of Fe–N–G, P–G and Pt/C in O_2-saturated (solid line) or N_2-saturated (dashed line) PBS medium at a scan rate of 1 mV s^{-1}.

3.3. MFCs performance

In order to investigate the performance of power production in the three types of MFCs, electrode potentials and power density curves were obtained at each external resistance when a steady voltage reached. As shown in Fig. 5A, the highest power density of 1149.8 mW m^{-2} was achieved by the Fe–N–G-MFC, while the P–G-MFC and the Pt/C-MFC produced much lower power densities of 109 mW m^{-2} and 561.1 mW m^{-2}, respectively. The anode and cathode potentials as a function of current density were measured to gain a better understanding of the contribution of individual electrode. It is obvious that cathode potentials followed the same trend as the power density curves, and anode potentials behaved similarly, providing evidence that the cathode performance was responsible for the differences in power production from these MFCs. Moreover, Pt/C and P–G with the relatively lower open circuit potential (OCP) of 0.11 V and 0.07 V, respectively, decreased very rapidly (Fig. 5B), resulting in poor performances of these MFCs. In contrast, the cathode potential with Fe–N–G was less affected (0.16 to −0.11 V), which implies that Fe–N–G can lower the overpotential for electrochemical reaction. Although the ORR

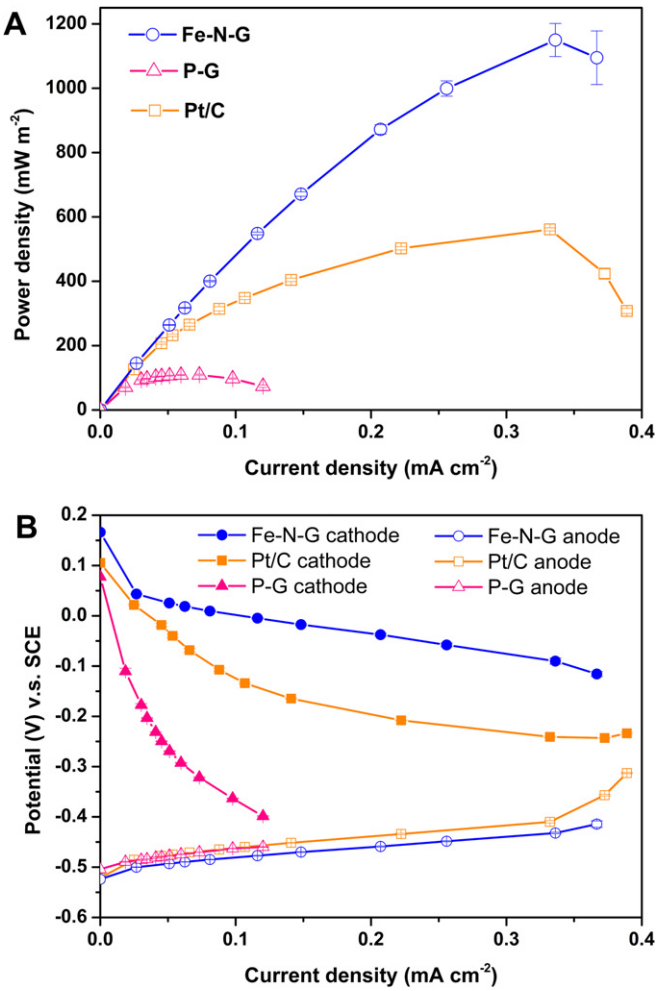

Fig. 5. Power density curves (A) and electrode potentials (B) for MFCs with different cathode catalysts.

electrocatalytic activity of the Fe–N–G electrode is lower than that of a commercial Pt/C electrode, the Fe–N–G-MFC significantly outperformed the Pt/C-MFC. This seems likely to be a consequence of a limitation to proton or oxygen transfer onto the catalyst layer at the air-cathode in the Pt/C-MFC, which is most possibly due to the poisoning of Pt [52] or increase of microbes on the surface of the cathode [53], resulting in relatively poor performance of the cell accordingly. Qu et al. [22] reported that the nitrogen-doped graphene catalyst showed a much better electrocatalytic activity and long-term operation stability than Pt for ORR. Hence, it appears that the Fe–N–G-cathode can also exhibit superior electrocatalytic activity and tolerance to biomass when it is equipped in an air-cathode MFC. On the basis of above results, it's clear that Fe–N–G can be used as an attractive alternative cathodic catalyst to Pt in MFCs.

The graphene-based catalyst prepared via a facile approach in this work significantly enhanced the MFC performance which exhibited 41% higher power output than that obtained in a previous study [54] (817 mW m^{-2}), where the sole iron tetrasulfophthalocyanine functionalized graphene was used as the cathodic catalyst. The better performance can be attributed to the formation of ORR active sites for pyridinic N, pyrrolic N and graphitic N [48], in addition to the effect of the incorporated iron. Further work is necessary to gain insight into the mechanisms of the oxygen reduction at the Fe–N–G catalyst in neutral medium and to optimize the performance of the system.

Regarding the effort to develop non-precious metal catalyst for ORR, pyrolyzed transition metal nitrogen-containing complexes supported on carbon (M–N–C, M = Fe, Co, Ni, etc.) have been widely explored for polymer electrolyte membrane fuel cells and considered the best promising catalysts due to its abundant availability and high electroactivity [55]. Since the excellent performance of the Fe–N–G-MFC was proved in present work (graphene as the novel carbon support), we believe that such a class of M–N–Graphene may be promising candidates for the future efficient and cost-effective catalysts in MFCs.

4. Conclusions

In summary, iron and nitrogen have been incorporated into graphene sheets to form an efficient non-precious metal catalyst applied to air-cathode MFCs. As-prepared Fe–N–G catalyst showed excellent ORR activity in neutral electrolytes, which could be attributed to the introduction of various nitrogen and iron components. The maximum power density of Fe–N–G-MFC (1149.8 mW m^{-2}) is ~2.1 times of that generated with the Pt/C-MFC and much higher than that of the P–G-MFC. These results suggest that the Fe–N–G catalyst promises to be a superb alternative to the costly Pt catalyst for practical application of MFCs.

Acknowledgments

The authors gratefully acknowledge the financial support provided by the National Natural Science Fund of China (No. 20977032).

References

[1] B.E. Logan, Nat. Rev. Microbiol. 7 (2009) 375–381.
[2] D.R. Lovley, Nat. Rev. Microbiol. 4 (2006) 497–508.
[3] K. Rabaey, R.A. Rozendal, Nat. Rev. Microbiol. 8 (2010) 706–716.
[4] F. Zhao, F. Harnisch, U. Schrorder, F. Scholz, P. Bogdanoff, I. Herrmann, Environ. Sci. Technol. 40 (2006) 5193–5199.
[5] F. Harnisch, U. Schroder, Chem. Soc. Rev. 39 (2010) 4433–4448.
[6] L.Y. Feng, Y.Y. Yan, Y.G. Chen, L.J. Wang, Energy Environ. Sci. 4 (2011) 1892–1899.
[7] S. Cheng, H. Liu, B.E. Logan, Environ. Sci. Technol. 40 (2006) 364–369.
[8] L.X. Zhang, C.S. Liu, L. Zhuang, W.S. Li, S.G. Zhou, J.T. Zhang, Biosens. Bioelectron. 24 (2009) 2825–2829.
[9] Y. Yuan, J. Ahmed, S. Kim, J. Power Sources 196 (2011) 1103–1106.
[10] Y. Zhang, Y. Hu, S. Li, J. Sun, B. Hou, J. Power Sources 196 (2011) 9284–9289.
[11] L. Deng, M. Zhou, C. Liu, L. Liu, C. Liu, S. Dong, Talanta 81 (2010) 444–448.
[12] J.M. Morris, S. Jin, J.Q. Wang, C.Z. Zhu, M.A. Urynowicz, Electrochem. Commun. 9 (2007) 1730–1734.
[13] F. Zhao, F. Harnisch, U. Schroder, F. Scholz, P. Bogdanoff, I. Herrmann, Electrochem. Commun. 7 (2005) 1405–1410.
[14] E. HaoYu, S. Cheng, K. Scott, B. Logan, J. Power Sources 171 (2007) 275–281.
[15] Y. Yuan, S.G. Zhou, L. Zhuang, J. Power Sources 195 (2010) 3490–3493.
[16] F. Zhang, D. Pant, B.E. Logan, Biosens. Bioelectron. 30 (2011) 49–55.
[17] A.K. Geim, K.S. Novoselov, Nat. Mater. 6 (2007) 183–191.
[18] S. Wang, P.K. Ang, Z. Wang, A.L.L. Tang, J.T.L. Thong, K.P. Loh, Nano Lett. 10 (2009) 92–98.
[19] X. Wang, L. Zhi, K. Mullen, Nano Lett. 8 (2007) 323–327.
[20] Z.S. Wu, W.C. Ren, D.W. Wang, F. Li, B.L. Liu, H.M. Cheng, ACS Nano 4 (2010) 5835–5842.
[21] C.-H. Lu, H.-H. Yang, C.-L. Zhu, X. Chen, G.-N. Chen, Angew. Chem., Int. Ed. 48 (2009) 4785–4787.
[22] L.T. Qu, Y. Liu, J.B. Baek, L.M. Dai, ACS Nano 4 (2010) 1321–1326.
[23] D.W. Boukhvalov, M.I. Katsnelson, Nano Lett. 8 (2008) 4373–4379.
[24] X.L. Li, H.L. Wang, J.T. Robinson, H. Sanchez, G. Diankov, H.J. Dai, J. Am. Chem. Soc. 131 (2009) 15939–15944.
[25] K.P. Loh, Q. Bao, P.K. Ang, J. Yang, J. Mater. Chem. 20 (2010).
[26] D. Geng, Y. Chen, Y. Chen, Y. Li, R. Li, X. Sun, S. Ye, S. Knights, Energy Environ. Sci. (2011).
[27] L. Feng, Y. Chen, L. Chen, ACS Nano 5 (2011) 9611–9618.
[28] E. Yeager, Electrochim. Acta 29 (1984) 1527–1537.
[29] M. Chatenet, M. Aurousseau, R. Durand, F. Andolfatto, J. Electrochem. Soc. 150 (2003) D47–D55.
[30] J. Chlistunoff, J. Phys. Chem. C 115 (2011) 6496–6507.
[31] M. Lefèvre, E. Proietti, F. Jaouen, J.-P. Dodelet, Science 324 (2009) 71–74.
[32] H.R. Byon, J. Suntivich, Y. Shao-Horn, Chem. Mater. 23 (2011) 3421–3428.
[33] N.I. Kovtyukhova, P.J. Ollivier, B.R. Martin, T.E. Mallouk, S.A. Chizhik, E.V. Buzaneva, A.D. Gorchinskiy, Chem. Mater. 11 (1999) 771–778.
[34] W.S. Hummers, R.E. Offeman, J. Am. Chem. Soc. 80 (1958) 1339.
[35] A. Thomas, A. Fischer, F. Goettmann, M. Antonietti, J.-O. Muller, R. Schlogl, J.M. Carlsson, J. Mater. Chem. 18 (2008) 4893–4908.
[36] S. Cheng, H. Liu, B.E. Logan, Electrochem. Commun. 8 (2006) 489–494.
[37] X. Wang, S.A. Cheng, Y.J. Feng, M.D. Merrill, T. Saito, B.E. Logan, Environ. Sci. Technol. 43 (2009) 6870–6874.
[38] H. Liu, B.E. Logan, Environ. Sci. Technol. 38 (2004) 4040–4046.
[39] D.R. Lovley, E.J.P. Phillips, Appl. Environ. Microbiol. 54 (1988) 1472–1480.
[40] H.L. Guo, X.F. Wang, Q.Y. Qian, F.B. Wang, X.H. Xia, ACS Nano 3 (2009) 2653–2659.
[41] M. Choucair, P. Thordarson, J.A. Stride, Nat. Nanotechnol. 4 (2009) 30–33.
[42] K.N. Kudin, B. Ozbas, H.C. Schniepp, R.K. Prud'homme, I.A. Aksay, R. Car, Nano Lett. 8 (2007) 36–41.
[43] A.C. Ferrari, J. Robertson, Phys. Rev. B 64 (2001) 075414.
[44] S. Stankovich, D.A. Dikin, R.D. Piner, K.A. Kohlhaas, A. Kleinhammes, Y. Jia, Y. Wu, S.T. Nguyen, R.S. Ruoff, Carbon 45 (2007) 1558–1565.
[45] Y. Ma, L. Sun, W. Huang, L. Zhang, J. Zhao, Q. Fan, W. Huang, J. Phys. Chem. C 115 (2011) 24592–24597.
[46] D.H. Long, W. Li, L.C. Ling, J. Miyawaki, I. Mochida, S.H. Yoon, Langmuir 26 (2010) 16096–16102.
[47] F.d.r. Jaouen, J. Herranz, M. Lefèvre, J.-P. Dodelet, U.I. Kramm, I. Herrmann, P. Bogdanoff, J. Maruyama, T. Nagaoka, A. Garsuch, J.R. Dahn, T. Olson, S. Pylypenko, P. Atanassov, E.A. Ustinov, ACS Appl. Mater. Interfaces 1 (2009) 1623–1639.
[48] K. Gong, F. Du, Z. Xia, M. Durstock, L. Dai, Science 323 (2009) 760–764.
[49] T.C. Nagaiah, S. Kundu, M. Bron, M. Muhler, W. Schuhmann, Electrochem. Commun 12 (2010) 338–341.
[50] S. Maldonado, K.J. Stevenson, J. Phys. Chem. B 109 (2005) 4707–4716.
[51] P. Wang, Z. Wang, L. Jia, Z. Xiao, Phys. Chem. Chem. Phys. 11 (2009) 2730–2740.
[52] F. Zhao, R.C.T. Slade, J.R. Varcoe, Chem. Soc. Rev. 38 (2009) 1926–1939.
[53] A.E. Tugtas, P. Cavdar, B. Calli, Bioresour. Technol. 102 (2011) 10425–10430.
[54] Y. Zhang, G. Mo, X. Li, J. Ye, J. Power Sources 197 (2012) 93–96.
[55] G. Wu, K.L. More, C.M. Johnston, P. Zelenay, Science 332 (2011) 443–447.